ARTICLES
PUBLISHED ONLINE: 12 SEPTEMBER 2010 | DOI: 10.1038/NGEO947
nature geoscience

Opposing decadal changes for the North Atlantic meridional overturning circulation

M. Susan Lozier[1]*, Vassil Roussenov[2], Mark S. C. Reed[1] and Richard G. Williams[2]*

The hydrographic properties of the North Atlantic Ocean changed significantly from 1950 to 2000: the subtropics warmed and became more saline, whereas the subpolar ocean cooled and freshened. These changes directly affect the storage of heat and fresh water in the ocean, but their consequences for ocean dynamics are determined by the resultant changes in seawater density. Here we use historical hydrographic data to show that the overall seawater density in the North Atlantic basin decreased during this 50-year period. As a result of these density changes, sea-surface heights changed in a spatially varying pattern with typical rates of 2 mm yr^{-1}, in broad agreement with tide-gauge measurements. Melding the observed density fields within a numerical model we find a slight weakening in the overturning of the subtropical gyre by -1.5 ± 1 Sv and a slight strengthening in the overturning of the subpolar gyre by $+0.8 \pm 0.5$ Sv. These gyre-specific changes run counter to the canonical notion of a single, basin-scale overturning cell and probably reflect interannual and decadal trends rather than any long-term climate trend. We conclude that gyre dynamics strongly affect temperature and salinity changes that translate into changes in the meridional overturning circulation.

The importance of the ocean in our climate system has been highlighted by recent studies illustrating its capacity as a heat, freshwater and carbon reservoir. In particular, the deep ocean has been shown to be a reservoir for anthropogenic carbon dioxide[1], with the deep limb of the meridional overturning circulation (MOC) apparently responsible for ventilating the deep waters with this tracer. The capacity for the deep ocean to continue to act as a reservoir for heat and carbon is critically dependent on this overturning circulation. As studies have revealed the warming of the global ocean's waters[2,3] and freshening at high latitudes[4–6], concern has mounted that these property changes are impacting the ocean's density field such that the MOC might slow[7,8], though the timing of this reduction remains unclear.

Measurements from the UK RAPID array along 26.5° N since 2004 are providing current estimates of the MOC (ref. 9), yet assessments of the long-term behaviour of the MOC remain elusive. Continuous time series from the RAPID array have shown that intra-annual variability of the MOC swamps interannual variability at this latitude, thus estimates of MOC change on the basis of synoptic surveys separated by years and decades[10,11] are unlikely to represent a realistic long-term trend. Unfortunately, modelling studies focused on temporal changes in the MOC in the North Atlantic have, so far, formed no consensus on either the magnitude or the sign of MOC changes in the North Atlantic[12]. Further confounding an assessment of past MOC changes, recent modelling studies have called into question the canonical picture of a single, basin-scale, overturning cell in the North Atlantic[13–15]. Results from these modelling experiments, which yield gyre-specific MOC changes, resonate with a past study of historical hydrographic data that showed pronounced gyre-specific changes in the North Atlantic property fields from 1950 to 2000 (ref. 16). Collectively, these studies suggest that an assessment of the North Atlantic MOC should consider latitudinal variations within the basin and that an inquiry into the linkage between gyre-specific property changes and MOC changes is warranted.

Towards this end, we estimate past changes in the MOC by using all hydrographic data collected from 1950 to 2000 over the entire North Atlantic basin. We are interested in identifying the spatial and temporal pattern of density change in this basin, the relative contribution of temperature and salinity to this change, and, importantly, the basin-wide MOC pattern that is dynamically consistent with these changes. Owing to uncertainties with the calculation of the MOC from the density field alone, we carry out this calculation within the context of a dynamical model to ensure that the velocity fields are dynamically consistent. Our goal with this study is to expand the spatial and temporal domain of past MOC estimates to provide a broader context for the interpretation of modelling and observational estimates of overturning in the North Atlantic.

North Atlantic property changes

For this investigation, we use historical hydrographic station data (pressure, salinity and temperature) collected between 1950 and 2000 (refs 17,18; Fig. 1a). Relatively sparse hydrographic data before the 1950s, and the sizeable temporal lag in the reporting and recording of more recent data, effectively dictates this temporal domain. The constraints imposed by data density—even in this most measured basin—limit our analyses of property changes over the past 50 years to two options: first, we sacrifice spatial resolution to analyse time series (from 1950 to 2000) of property changes averaged over the central subtropical and subpolar basins (Fig. 1a); second, we maintain the spatial resolution of the data and restrict our analysis of temporal change to two time periods, as explained below.

Salinity and temperature changes over the past 50 years exhibit strong variability in both the subtropical and subpolar basins (Fig. 1b,c) at a representative depth of 1,000 m. The strong interannual variability of the subtropical property changes stands in sharp contrast to the nearly decadal variability of the subpolar gyre, variability that is more easily mapped onto the broad temporal change of the North Atlantic Oscillation (NAO) index from the 1950s and

[1]Division of Earth and Ocean Sciences, Nicholas School of the Environment, Duke University, Durham, North Carolina 27708, USA, [2]Department of Earth and Ocean Sciences, Liverpool University, Liverpool L69 3GP, UK. *e-mail: mslozier@duke.edu; ric@liverpool.ac.uk.

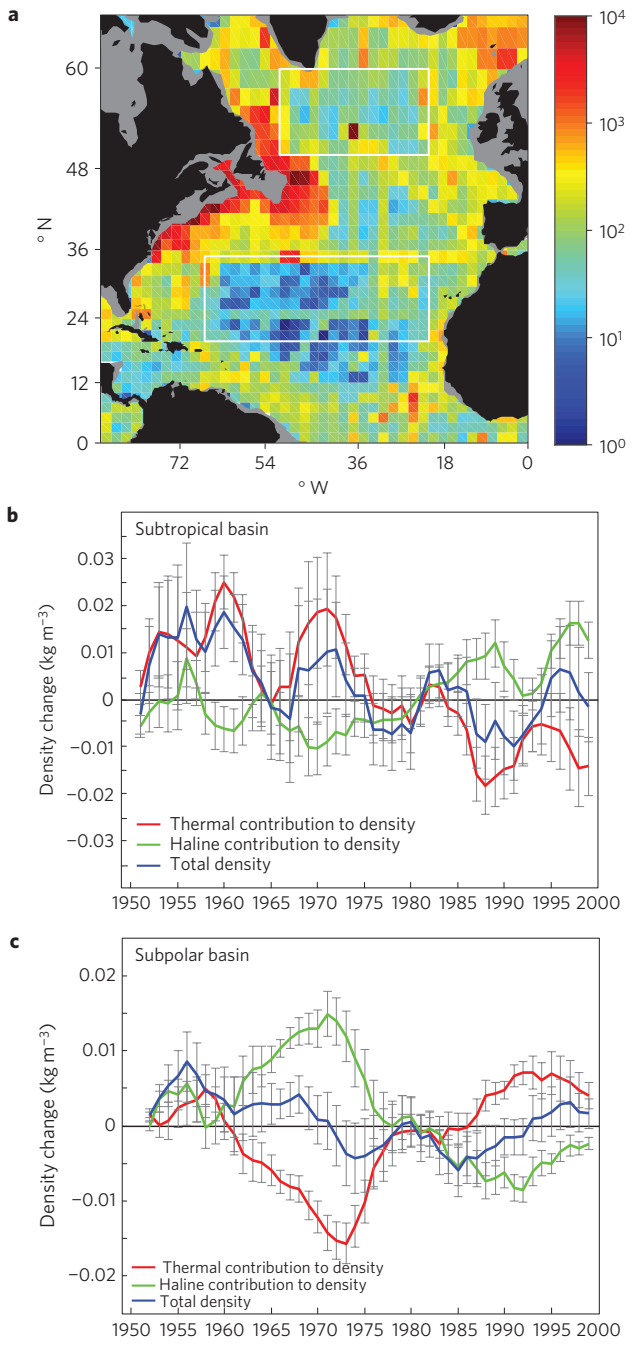

Figure 1 | Historical hydrographic data analysis. a, Number of stations per 2° × 2° bin, totalling 508,157: 44,343 from 1950 to 1959; 86,556 from 1960 to 1969; 138,237 from 1970 to 1979; 146,753 from 1980 to 1989; 92,268 from 1990 to 1999. Outlined are the subtropical (11,174 stations) and subpolar domains (37,346 stations) used to construct Fig. 1b,c. Bathymetry <200 m is shaded grey. **b**, Thermal and haline contributions to density[32] and their sum averaged over the area outlined in Fig. 1a, at a depth of 1,000 m. Error bars depict standard errors of the quality-controlled data[33]. **c**, The same as **b**, except for the central subpolar basin.

1960s—when it was relatively low—compared to the 1980s and 1990s—when it was relatively high[19,20]. Also revealed from these property changes is the tendency for density compensation in both basins, but particularly so for the subpolar basin where the haline contribution to density is of comparable magnitude to the thermal component. In general, when the waters freshened they cooled, and, likewise, when they became saltier they warmed.

Decomposition of these property changes into the component due to water-mass change and that due to heaving of the isopycnals reveals that the subpolar property changes are largely the result of water-mass changes, whereas the subtropical changes can be largely attributed to wind-induced heaving of isopycnals over time. In spite of the compensation between salinity and temperature, both basins exhibit significant changes in density at a depth of 1,000 m: a decreasing trend is noted for both the subtropical ($-3.3 \times 10^{-4} \pm 6.5 \times 10^{-5}$ kg m^{-3} yr^{-1}) and subpolar regions ($-1.3 \times 10^{-4} \pm 3.0 \times 10^{-5}$ kg m^{-3} yr^{-1}), although the linear change accounts for only 36 and 29% of the variance in the density change for the subtropical and subpolar basins, respectively. Clearly, these statistics, coupled with an inspection of the time series in Fig. 1 and those for other surfaces (Supplementary Fig. S1), cast doubt on our ability to meaningful interpret the 50-year change as part of a longer-term trend. Nonetheless, the property changes over this 50-year period are significant and of interest to place the dynamical impacts of predicted trends in freshening or warming in the context of strong interannual and decadal variability.

Given the constraints of data availability and distribution, an examination of basin-wide spatial patterns of temperature, salinity and density is accomplished by averaging the historical hydrographic data for two separate periods (1980–2000 and 1950–1970; see Supplementary Fig. S2 for data coverage) with known differences in wind and buoyancy forcing, as represented by the NAO index[19]. Though this choice will obscure the impact of the higher-frequency property changes in the subtropical basin, the goal is to yield insight into the property fields of the North Atlantic under two different, known and prominent forcing states. From the property changes shown in Fig. 2 for two composite layers, a picture of compensated, spatially varying anomalies emerges: the subpolar gyre is generally cooler and fresher in the latter time period, whereas the subtropical gyre and the tropics are generally warmer and more saline. In particular, there is a striking division in the property changes at the subtropical gyre–subpolar gyre boundary, as noted earlier in a study of heat-content changes in this basin[16], and more clearly pronounced when the property changes are zonally averaged (Supplementary Fig. S3). This sharp gyre demarcation suggests a strong role for basin-scale dynamics in setting these patterns.

Given the temperature and salinity changes specific to each gyre, an overall density decrease means that the freshening has outpaced the cooling in the subpolar gyre, whereas the warming has outpaced the salinification in the subtropical gyre. It is important to note that the density change is reduced from what we would estimate on the basis of an analysis of temperature alone or salinity alone, and that the similar density tendency in both basins leads to maps of density change (Fig. 2) lacking in gyre specificity. Overall, the analysis of these property changes reveals strong spatial and temporal variability over the 50-year period from 1950 to 2000: most striking is the spatial divide between the subtropical and subpolar gyres, and the temporal divide between the periods of sustained weak and strong NAO forcing.

Impact of density changes on sea level

What are the consequences of these density changes? A direct impact of density change is sea-level change. A map of the rate of sea-level rise evaluated from the former to the latter 20 year time period reveals a general rise in sea level, reaching 3–4 mm yr^{-1} in the mid-latitudes (Fig. 3). This rise in sea level is broadly comparable to reconstructions of sea-level rise between 1950 and 2000 on the basis of tide-gauge data, where sea-level rise reaches a peak of typically 3 mm yr^{-1} along 40° N[21]. However, this regional pattern should not simply be viewed in terms of a persistent trend, because sea level seems to fall along 40° N between 1993 and 2003 at a rate reaching −10 mm yr^{-1} (ref. 22). Hence, the regional pattern

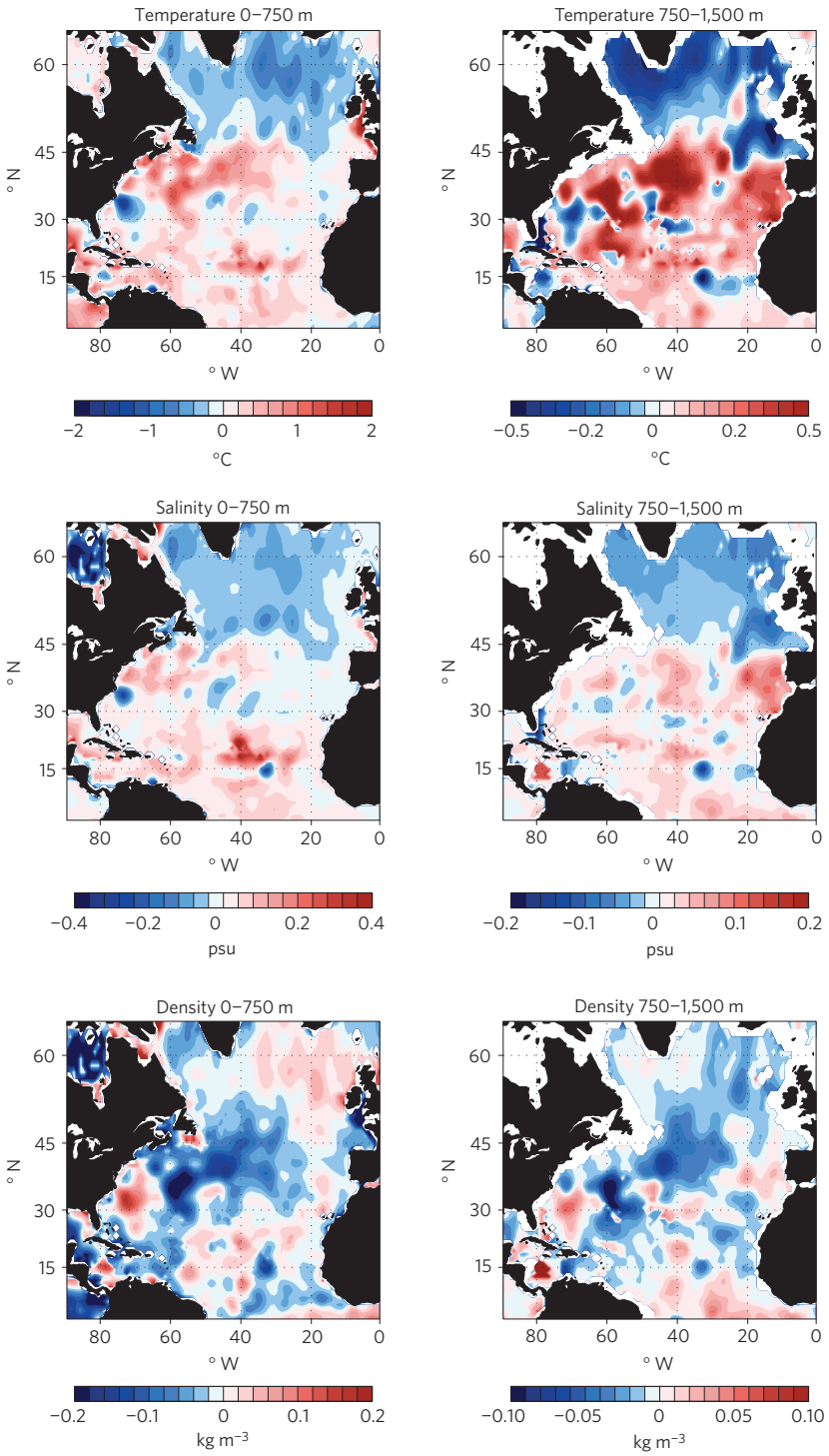

Figure 2 | Spatial fields of temperature, salinity and density changes. Data are binned using a 2° × 2° horizontal grid for the composite layers of 0–750 m and 750–1,500 m: the 1980–2000 time period minus the 1950–1970 time period. Red indicates warming, salinification and densification, whereas blue indicates cooling, freshening and de-densification; note the larger ranges used for the upper waters. Data are plotted after a nine-point smoothing is applied.

of sea-level change seems to be affected by natural variability, in a manner similar to ocean heat content[16], as well as by longer-term climate change.

These diagnosed sea-surface-height changes reflect different and, sometimes, opposing contributions from temperature and salinity changes: the thermal contribution provides a reduction over the subpolar gyre and a rise over the subtropical gyre, particularly its northern flank (Fig. 3b), whereas the salinity contribution provides a more uniform rise in sea level over the subpolar gyre and much of the subtropical gyre, with localized reduction over the tropics (Fig. 3c). The mean rate of sea-level rise of 0.25 ± 3.12 mm yr^{-1}, with comparable temperature and salinity contributions of 0.26 ± 3.56 and 0.25 ± 3.32 mm yr^{-1}, respectively, reveals the dominance of regional variability over basin-averaged changes; see Supplementary Fig. S4 for an estimate of sea-level change that includes changes in the mass field as well as steric effects.

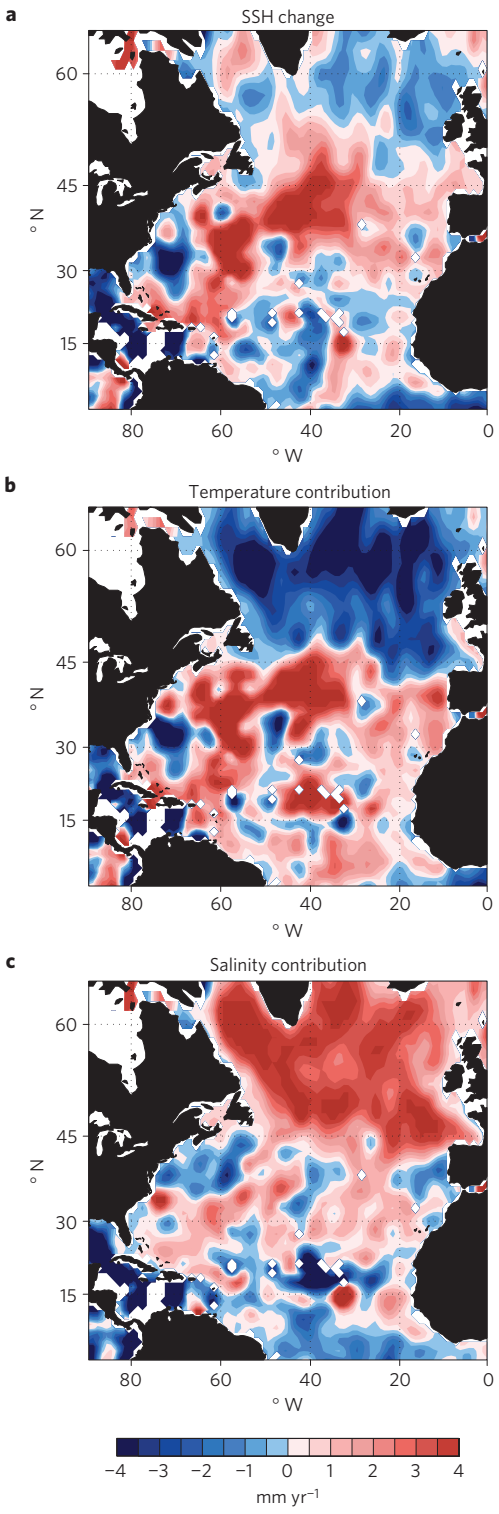

Figure 3 | Sea-surface height changes. a, Rate of sea-surface-height change (mm yr^{-1}) between the 1980–2000 and 1950–1970 periods (red is an increase in time, blue is a decrease) on the basis of the density fields for each period. **b**, Temperature contribution to the estimate in **a**. **c**, Salinity contribution to the estimate in **a**. The basin-mean rates of sea-level rise from the temperature and salinity contributions are 0.26 ± 3.56 and 0.25 ± 3.32 mm yr^{-1}, respectively.

Impact of density changes on the MOC

The dynamical consequence of property changes for the MOC depends on the zonal contrast in density: the difference in density between the western and eastern boundaries of the basin is directly linked to the strength of the MOC (refs 23,24). Indeed, the measurement of density along these boundaries has formed a central part of the ongoing daily monitoring of the overturning along 26° N since 2004 (refs 9,25). Not surprisingly, for our analysis of density changes between the two 20-year periods, there are insufficient boundary data to provide a robust estimate of the overturning. Rather than ignore any dynamical implications, we explore the possibility that the interior density field has been sufficiently sampled to constrain a model assessment of the overturning. Our approach is as follows: for each 20 year period, the average temperature and salinity fields at 1° horizontal resolution are used to initialize the MIT circulation model over the North Atlantic[26]; temperature and salinity from a global inverse model[27] are used to initialize the rest of the domain. After initialization, the circulation model is integrated for 18 months to enable the density field to dynamically adjust through boundary waves propagating around the basin[28]. The MOC streamfunction is then calculated from these adjusted fields. This method was tested using output from a global inverse model by comparing the MOC reconstructed from the model's density field with the model 'truth', namely the MOC calculated with the model's velocity field. The favourable comparison (Supplementary Fig. S5a) lends credence to our method and suggests that hydrographic observations should be an important constraint on state-estimate models.

Using the historical hydrographic data, the average MOC for the two time periods reveals the expected structure: northward transport of light water replaced at depth with a southward transport of dense water (Fig. 4a). The overturning transport reaches a maximum of ~16 Sv at around 45° N, with the transport changing sign near a depth of 1,300 m. The difference between the estimates for these two time periods (Fig. 4b) reveals a gyre-specific pattern: the overturning during the latter time period is slightly weaker over the subtropical gyre by −1.5 Sv, but slightly stronger over the subpolar gyre by typically 0.5 Sv. The weaker overturning for the subtropical gyre is concomitant with a weakening of the east–west density gradient in the thermocline waters (Fig. 5a). This weakening results from the westward warming over the upper 1,500 m (Fig. 2), producing a thickening of the thermocline, a rise in sea level and a reduction in the northward velocity shear, the latter consistent with the model prediction of a slight weakening in the overturning. Over the subpolar gyre, there is a more complicated picture (Fig. 5a): the westward freshening over the upper 500 m actually suggests a weakening in the east–west density gradient and a decrease in the northward velocity shear, whereas the eastward freshening at depth suggests a strengthening in the east–west density gradient and an increase in the northward velocity shear; see Fig. 2c and Supplementary Fig. S6c. The latter process dominates in the model adjustment, leading to a slight strengthening in the overturning. The impact of these changes in the lower thermocline argues for full-depth measures of the density field to accurately assess overturning changes.

The robustness of the estimate for the overturning, and indeed the noted changes in the overturning circulation, depends crucially on the representativeness of the hydrographic data used to initialize the model integration. To assess the effect of data uncertainties on the overturning estimate, multiple integrations of the model are run, all identical save for the initial fields, which are selected randomly on the basis of the standard errors for the density field for each time period. The collection of these ensemble runs (Fig. 4c) qualitatively shows the envelope of possible overturning changes given the errors in the density field, but also yields a quantitative measure of the robustness of the overturning estimate (Fig. 4d): the overturning has weakened over the subtropical gyre by -1.5 ± 1 Sv, but strengthened over the subpolar gyre by 0.8 ± 0.5 Sv.

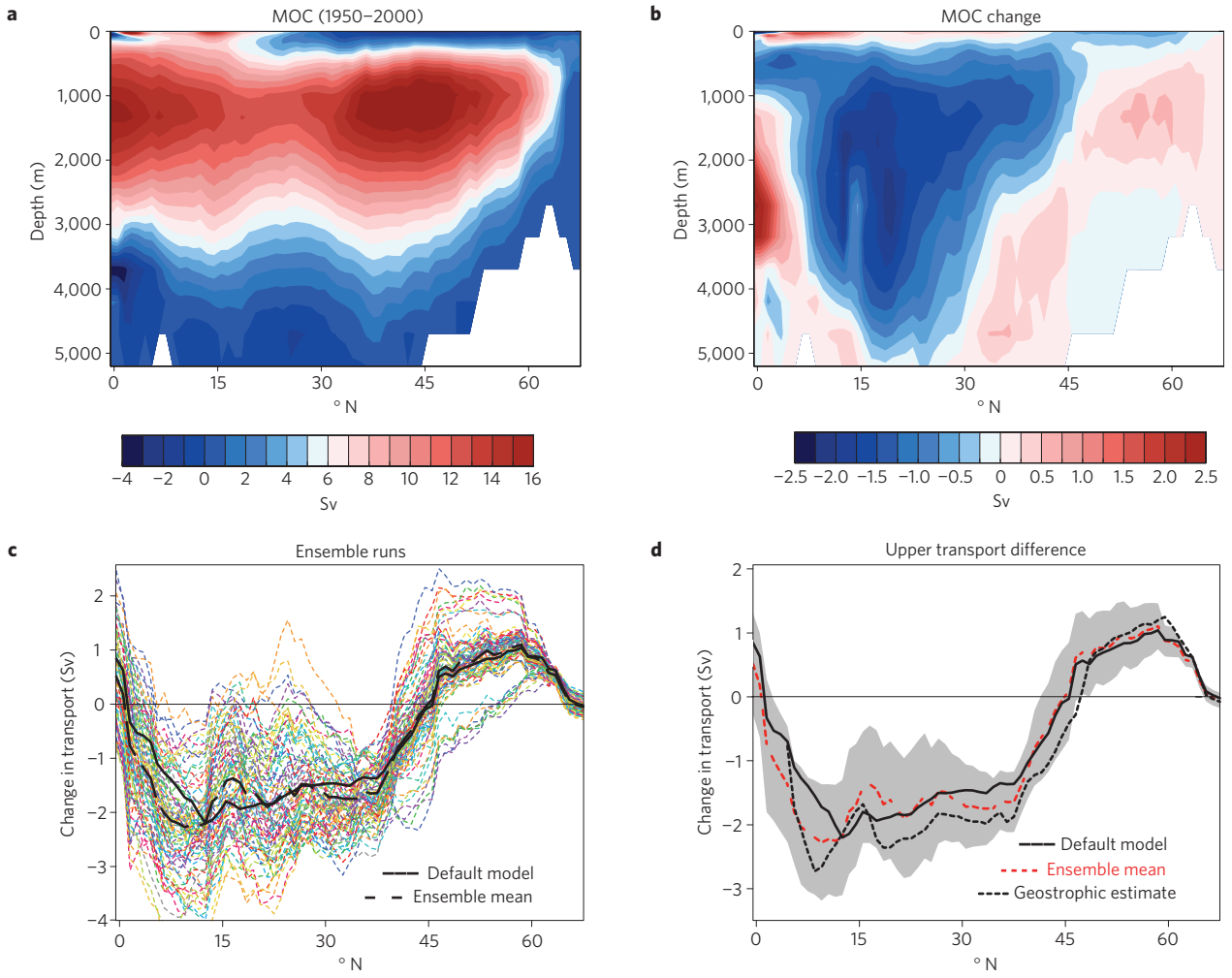

Figure 4 | Changes in the meridional overturning circulation. a, Estimate of the mean MOC streamfunction (Sv) evaluated from the MIT model initialized with historical hydrographic data averaged from 1950 to 2000. **b**, Change in MOC (Sv) from 1950–1970 to 1980–2000. **c**, 80 ensemble estimates of the MOC change (Sv), evaluated from 100 m to 1,300 m. **d**, Change in MOC (Sv) calculated with the default model (solid line), calculated from geostrophic velocities derived from adjusted density fields (dotted line) and calculated as the average (dashed line) of the ensembles shown in **c**. Grey shading outlines one standard deviation from the mean of the ensembles.

Also evident in Fig. 4d is that the estimate of the overturning on the basis of the adjusted density field is remarkably similar to that calculated from the model's velocity field, underscoring the overriding importance of the geostrophic velocity field (Fig. 5b) to the overturning circulation. Although the winds are ultimately important in affecting the density distribution over the two 20-year periods, the MOC differences are relatively insensitive to the choice of winds during the short dynamical adjustment used to estimate the overturning (Supplementary Fig. S7).

Overshadowing in importance the magnitude of these estimated MOC changes is their spatial pattern: the canonical picture of MOC changes extending over the entire North Atlantic basin does not seem to hold. Instead, MOC changes are found to be gyre specific, in agreement with independent model experiments[13–15], but not yet realized with observations. Indeed, this gyre-scale pattern mimics that found by comparing model runs that differ only in their wind forcing[13], strongly suggesting that the observed overturning changes estimated here are primarily attributable to the different density distributions arising from contrasting wind forcing between high- and low-NAO periods. Modelling studies lead us to expect basin-wide MOC changes only when buoyancy forcing dominates, presumably on longer timescales than the interannual and decadal timescales afforded by the current observational database.

An intriguing question is the mechanism by which the property and overturning changes could be causally related. Given the paradigm of high-latitude buoyancy forcing producing basin-wide overturning changes, we would expect increases in ocean heat content in the subtropical gyre to result from a strengthening in the overturning. Paradoxically, the reverse holds: heat-content gain in the latter period is associated with a weakening in the subtropical overturning. Such an association is explained causally: anomalous wind forcing associated with the positive NAO state leads to a deepening of the subtropical thermocline through increased Ekman pumping, which in turn leads to a redistribution of heat in the basin and a gain in heat content over the subtropical gyre[16,28]. Wind-induced redistributions of heat, as well as those of freshwater, that alter the west–east contrast in density across the basin will then impact the MOC. With this causal link, the overturning circulation is not driving the property changes, but is instead responding to them. Clearly, this causality needs to be tested with long-term measurements of property and overturning changes, as well as a dynamical model that can realistically link the two.

Finally, though recent interest in the MOC has focused on the possibility of long-term trends due to changes in buoyancy forcing, identifying this signal is problematic and challenging. This study emphasizes how property changes and overturning

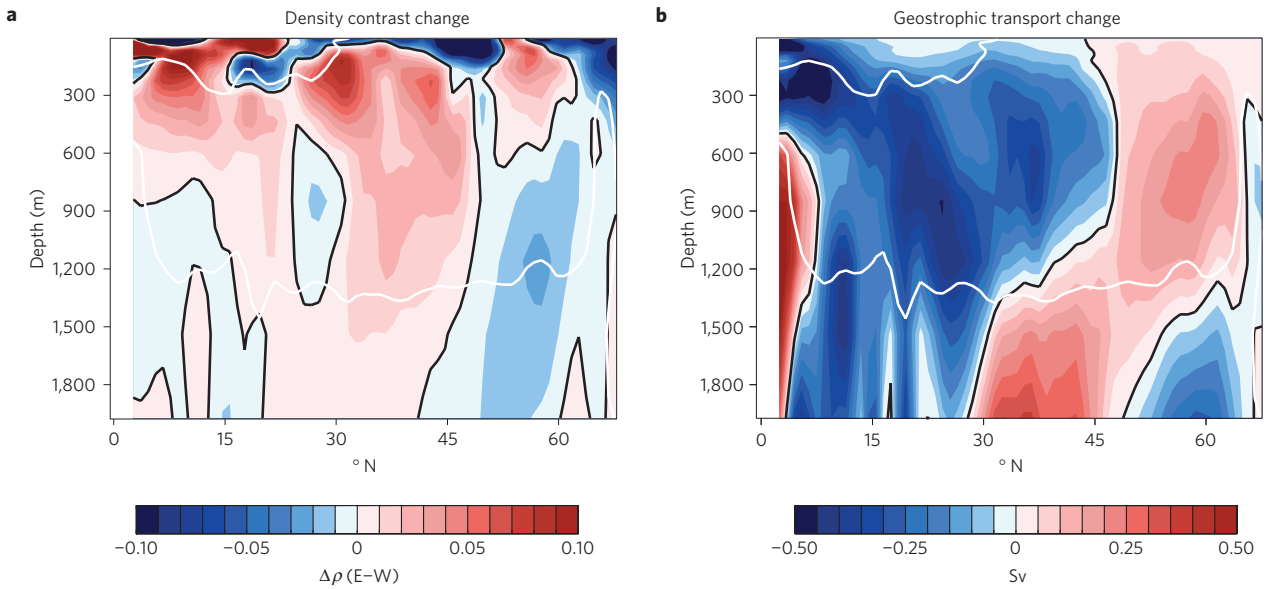

Figure 5 | Relationship of MOC changes to observed density field. a, Density difference (kg m^{-3}) between the eastern and western boundaries in the model fields after 18 months of forward integration and dynamical adjustment. A weakening (red) in the density contrast is consistent with reduced vertical shear in northward velocity, whereas a strengthening (blue) indicates increased vertical shear. **b**, Change in geostrophic transport (Sv) for each depth bin from the latter to the former time period after 18 months of model integration. Thick white lines on both panels are zero contours of the meridional transport, positive above typically 1,300 m.

changes are gyre specific. Thus, the MOC variability[9] measured at 26° N might only be representative of changes in the subtropical gyre, as suggested by the MOC reconstructed at 41° N from ARGO data[29] and inferred along the North American east coast from sea-level variability[30]. Furthermore, the recent reversal of property trends in the subpolar basin[6,31] suggests that a corresponding reversal of the overturning pattern reported here is perhaps underway. Given the increasing availability of density data, it should soon be possible to estimate the spatial and temporal variability of the MOC in more detail, a necessary goal before a reliable assessment of anthropogenic-induced trends can be made.

Received 6 April 2010; accepted 29 July 2010; published online 12 September 2010; corrected online 14 October 2010

References

1. Sabine, C. L. *et al.* The oceanic sink for anthropogenic CO_2. *Science* **305,** 367–371 (2004).
2. Levitus, S., Antonov, J. I., Boyer, T. P. & Stephens, C. Warming of the world ocean. *Science* **287,** 2225–2229 (2000).
3. Levitus, S., Antonov, J. & Boyer, T. Warming of the world ocean, 1955–2003. *Geophys. Res. Lett.* **32,** L02604–L02607 (2005).
4. Dickson, B. *et al.* Rapid freshening of the deep North Atlantic Ocean over the past four decades. *Nature* **416,** 832–837 (2002).
5. Curry, R., Dickson, B. & Yashayaev, I. A change in the freshwater balance of the Atlantic Ocean over the past four decades. *Nature* **426,** 826–829 (2003).
6. Boyer, T. *et al.* Changes in freshwater content in the North Atlantic Ocean 1955–2006. *Geophys. Res. Lett.* **34,** L16603–L16607 (2007).
7. Bi, D., Budd, W. F., Hirst, A. C. & Wu, X. Collapse and reorganisation of the Southern Ocean overturning under global warming in a coupled model. *Geophys. Res. Lett.* **28,** 3927–3930 (2001).
8. Gregory, J. M. *et al.* A model intercomparison of changes in the Atlantic thermohaline circulation in response to increasing atmospheric CO_2 concentration. *Geophys. Res. Lett.* **32,** L12703–L12707 (2005).
9. Cunningham, S. A. *et al.* Temporal variability of the Atlantic meridional overturning circulation at 26.5° N. *Science* **317,** 935–938 (2007).
10. Bryden, H. L., Longworth, H. R. & Cunningham, S. A. Slowing of the Atlantic meridional overturning circulation at 25 N. *Nature* **438,** 655–657 (2005).
11. Lumpkin, R., Speer, K. G. & Koltermann, K. P. Transport across 48° N in the Atlantic Ocean. *J. Phys. Oceanogr.* **38,** 733–752 (2008).
12. Cunningham, S. A. & Marsh, R. Observing and modeling changes in the Atlantic MOC. *Wiley Interdiscip. Rev. Clim. Change* **1,** 180–191 (2010).
13. Biastoch, A., Böning, C. W., Getzlaff, J., Molines, J-M. & Madec, G. Causes of interannual–decadal variability in the meridional overturning circulation of the midlatitude North Atlantic Ocean. *J. Clim.* **21,** 6599–6615 (2008).
14. Bingham, R. J., Hughes, C. W., Roussenov, V. & Williams, R. G. Meridional coherence of the North Atlantic meridional overturning circulation. *Geophys. Res. Lett.* **34,** L23606–L23611 (2007).
15. Baehr, J., Stroup, A. & Marotzke, J. Testing concepts for continuous monitoring of the meridional overturning circulation in the South Atlantic. *Ocean Modelling* **29,** 147–153 (2009).
16. Lozier, M. S. *et al.* The spatial pattern and mechanisms of heat-content change in the North Atlantic. *Science* **319,** 800–803 (2008).
17. Boyer, T. *et al.* in *NOAA Atlas NESDIS 60* (ed. Levitus, S.) 190–190 (US Government Printing Office, 2006).
18. Gregory, D. N. Canadian Science Advisory Secretariat Research Document—2004/075 (2004).
19. Hurrell, J. W. Decadal trends in North Atlantic oscillation: Regional temperatures and precipitation. *Science* **269,** 676–679 (1995).
20. Hurrell, J. W., Kushnir, Y., Ottersen, G. & Visbeck, M. (eds) *The North Atlantic Oscillation: Climate Significance and Environmental Impact* (Geophysical Monograph Series 134, American Geophysical Union, 2003).
21. Church, J. A., White, N. J., Coleman, R., Lambeck, K. & Mitrovica, J. X. Estimates of the regional distribution of sea level rise over the 1950–2000 period. *J. Clim.* **17,** 2609–2625 (2004).
22. Church, J. *et al.* Understanding global sea levels: Past, present and future. *Sustain. Sci.* **3,** 9–22 (2008).
23. Marotzke, J. *et al.* Construction of the adjoint MIT ocean general circulation model and application to Atlantic heat transport sensitivity. *J. Geophys. Res.* **104,** 529–547 (1999).
24. Baehr, J., Hirschi, J. J. M., Beismann, J-O. & Marotzke, J. Monitoring the meridional overturning circulation in the North Atlantic: A model-based array design study. *J. Mar. Res.* **62,** 283–312 (2004).
25. Kanzow, T. *et al.* Observed flow compensation associated with the MOC at 26.5° N in the Atlantic. *Science* **317,** 938–941 (2007).
26. Marshall, J., Hill, C., Perelman, L. & Adcroft, A. Hydrostatic, quasi-hydrostatic, and nonhydrostatic ocean modeling. *J. Geophys. Res.* **102,** 5733–5752 (1997).
27. Koehl, A., Dommenget, D., Ueyoshi, K. & Stammer, D. *Ocean Synthesis.* Report No. 40, (2006). http://www.ecco-group.org/ecco1/report/report_40.pdf).
28. Roussenov, V. M., Williams, R. G., Hughes, C. W. & Bingham, R. J. Boundary wave communication of bottom pressure and overturning changes for the North Atlantic. *J. Geophys. Res.* **113,** C08042–C08053 (2008).
29. Willis, J. K. Can *in situ* floats and satellite altimeters detect long-term changes in Atlantic Ocean overturning? *Geophys. Res. Lett.* **37,** L06602 (2010).
30. Bingham, R. J. & Hughes, C. W. Signature of the Atlantic meridional overturning circulation in sea level along the east coast of North America. *Geophys. Res. Lett.* **36,** L02603–L02607 (2009).

31. Hatun, H., Sando, A. B., Drange, H., Hansen, B. & Valdimarsson, H. Influence of the Atlantic subpolar gyre on the thermohaline circulation. *Science* **309,** 1841–1844 (2005).
32. Fofonoff, N. P. & Millard, R. C. J. *Algorithms for Computation of Fundamental Properties of Seawater* Vol. 44, 53 (Unesco Technical Papers in Marine Science, 1985).
33. Lozier, M. S., Owens, W. B. & Curry, R. G. The climatology of the North Atlantic. *Prog. Oceanogr.* **36,** 1–44 (1995).

Acknowledgements

The authors gratefully acknowledge support from the US National Science Foundation and the UK Natural Environment Research Council.

Author contributions

M.S.L. led the data study and its interpretation and R.G.W. led the modelling study and interpretation. V.R. conducted the modelling study and developed the model-data analysis. M.S.C.R. conducted the historical-data analysis. M.S.L. and R.G.W. jointly wrote the paper.

Additional information

The authors declare no competing financial interests. Supplementary information accompanies this paper on www.nature.com/naturegeoscience. Reprints and permissions information is available online at http://npg.nature.com/reprintsandpermissions. Correspondence and requests for materials should be addressed to M.S.L. or R.G.W.

nature geoscience

SUPPLEMENTARY INFORMATION

DOI: 10.1038/NGEO947

Opposing decadal changes for the North Atlantic meridional overturning circulation

M. Susan Lozier[1], Vassil Roussenov [2], Mark S. C. Reed[1] and Richard G. Williams[2]

[1]*Division of Earth and Ocean Sciences, Nicholas School of the Environment, Duke University, Durham, NC 27708, USA*

[2]*Department of Earth and Ocean Sciences, Liverpool University, Liverpool, L69 3GP, UK*

Supplementary Information

Diagnosed sea-surface height changes

Density changes between the two 20-year periods, 1980-2000 and 1950-1970, are used to infer sea surface height change in two different ways:

1. Sea surface height, η, is estimated solely from the *in situ* density, ρ, according to:

$$\eta(x,y) = -\frac{1}{\rho_o}\int_{z=-D}^{z=0}\left(\rho - \rho_{ref}(z)\right)dz, \qquad \text{(S1)}$$

where $\rho_{ref}(z)$ is a reference density, calculated as the average density on each of the 20 depths over which the observational data is distributed, and ρ_o (1040 kg $m^{-3)}$ is the volume-weighted, basin-averaged density for the entire domain. This calculation is repeated for each of the 20-year periods; the difference in sea surface height for each twenty-year period is then divided by their

DOI: 10.1038/NGEO947

separation of 30 years to provide the rate of change in sea surface height due to steric effects. Note that this estimate does not include any regional contributions to the sea surface height change from a dynamical adjustment of mass or any contribution from changes in the volumetric supply from increased precipitation minus evaporation, ice melting or river runoff.

2. Sea surface height is also estimated for each 20-year period by initializing the MIT global circulation model with the North Atlantic data (together with global temperature and salinity taken from GECCO[27]), then diagnosing the sea surface height after either a short 5-day or a longer 1-year integration. The forward integration allows for the dynamic adjustment of the mass field. Sea level height changes calculated with this method include steric contributions as well as any contributions from a rapid, barotropic rearrangement of mass.

The data-based steric estimate of sea surface height change (Supplementary Fig. S4a) reveals an increase over most of the basin, particularly over the northern flank of the subtropical gyre, but also reveals local regions of decrease, particularly in the northeastern subpolar gyre and in parts of the tropics. The mean rate of sea level rise is 0.25 mm yr^{-1}, with a much larger standard deviation of 3.12 mm yr^{-1}. In comparison, estimates of sea level rise from tide gauge data show a broadly similar band of sea level rise over the northern flank of the subtropical gyre with values ranging from 2.0 to 3.5 mm yr^{-1} for the same period of 1950 to 2000[22].

The basin-scale pattern of the model estimate of sea surface height change is broadly similar to that for the data-based steric estimate, but there are local differences. Notably, this estimate produces a more pronounced fall of sea-surface height over the subpolar gyre (Supplementary

Fig. S4b). After a 5-day adjustment, the model estimate provides a slightly larger mean rate of sea level rise (0.44 mm yr^{-1}) over the entire basin, but has a smaller standard deviation (1.43 mm yr^{-1}). With a 1-year adjustment, the model estimate of sea surface height change reveals a similar basin-scale rise (0.54 mm yr^{-1}), but a smaller standard deviation (0.89 mm yr^{-1}) (Supplementary Fig. S4c).

The MIT global circulation model (79.5S - 79.5N) used for this study has a horizontal resolution of 1° with 23 levels in the vertical spaced 10m apart at the surface to 500m at depth. Model set-up is similar to the forward model set-up for GECCO (Koehl et al., 2006).

Model methodology to estimate MOC from the in situ density data

Changes in MOC can be estimated from boundary contrasts in pressure, which are inferred from measures of the surface pressure and *in situ* density using the hydrostatic relationship[23,24]; where the streamfunction for the meridional geostrophic velocity is given by:

$$\psi(y,z) = \frac{1}{\rho_o f}\int_z^{\eta} (P_e - P_w)dz \quad , \qquad \text{(S2)}$$

η is the height of the sea surface, z is the vertical position, P_e and P_w are the bottom pressures on the eastern and western boundaries, respectively, ρ_o is a reference density and f is the Coriolis parameter.

While the data reveals basin-scale changes in density between the two 20-year periods (Fig. 2c), there is insufficient data along the boundaries to resolve the geostrophic overturning. Given this limitation, we instead choose to meld the data with the global, MIT general circulation model[26] for each of the separate 20-year periods. The procedure is as follows:

DOI: 10.1038/NGEO947

i. The model is initialized with the observed temperature and salinity data over the North Atlantic on a 1-degree grid on 23 depth levels (with the data linearly interpolated in the vertical) and after a nine-point smoothing is applied (as in Fig. 2).

ii. The model is initialized over the rest of the globe using temperature and salinity data from a global inverse model[27], which is averaged for the appropriate 20-year period taken from a 1952-2001 reconstruction.

iii. The model is integrated forward in time with monthly forcing taken from monthly-mean wind stresses from NCEP averaged over the appropriate 20-year period. The three-dimensional temperature and salinity fields are relaxed to the initial annual-averaged temperature and salinity data on a 3-year timescale.

iv. The MOC estimate is based on model fields after a dynamical adjustment of 18 months. The fields over an entire seasonal cycle from 6 to 18 months are averaged to compute the MOC. See below for an explanation of how this time scale was chosen. This procedure to estimate the MOC is a compromise between allowing the model sufficient time to dynamically adjust, via the propagation of boundary waves around the boundary, and minimizing the drift of the model temperature and salinity away from the initial data.

How does our algorithm for estimating the MOC compare with an independent 'model truth'?

A test of our algorithm for the estimation of MOC changes is applied using a global inverse model, GECCO[27]. Model density fields are used to produce MOC estimates from the method described above. These estimates are then compared with the MOC changes diagnosed directly from the model's monthly velocity field (Supplementary Fig. S5a, crosses). For this comparison, the MIT model is initialized with temperature and salinity data taken from 20-year averages from GECCO, then integrated forward, incorporating the NCEP wind forcing and background relaxation.

The MOC estimates vary with the length of the model integration (Supplementary Fig. S5a, lines), except near 45^{o}N, where the adjustment timescale does not strongly affect the estimate. The best match between the estimate based on the property fields and that calculated directly from the velocity fields occurs for a model integration of one year. Thus, MOC estimates using an initialization with the observed property fields were calculated using modeled fields averaged from 6 to 18 months following initialization.

How do our estimates for the MOC differ according to whether the density data is taken from GECCO or from historical data?

The reconstruction of the overturning from the GECCO monthly velocities shows an overall strengthening between the two periods, 1950-1970 to 1980-2000, over the entire basin north of 20^{o}N, reaching 2.8 Sv at 45^{o}N (Supplementary Fig. S5a crosses). This response is also seen when diagnosing the MOC from GECCO density data (Supplementary Fig. S5a, black line). In contrast, when our algorithm is applied using historical density data, MOC changes have a different structure: the MOC weakens over the subtropical gyre south of 45^{o}N and strengthens

DOI: 10.1038/NGEO947

north of there. These different MOC responses can be attributed to the difference between the temperature, salinity and density changes in GECCO and the corresponding changes in the observations.

How is our algorithm for estimating the MOC affected by density observations at the boundary?

Overturning is estimated as above, but with one change: Density data specific to each time period is removed from within 1^{o} of the topography over the entire basin (Supplementary Fig. S5b) and replaced with climatological data. The resulting overturning is still close to the GECCO truth (Supplementary Fig. S5b, crosses) with the maximum MOC change reduced from 2.8 Sv to 2.4 Sv. When data is removed within 2^{o} of the topography, the overall pattern is also maintained, though the MOC change is reduced further by ~0.2 Sv.

When historical data is used to compute the MOC change with boundary data removed (as described above), the overturning pattern remains much the same with only a slight shift in the magnitudes by up to 0.3 Sv in the subtropical basin (Supplementary Fig. S5c).

How have the model estimates of temperature and salinity adjusted?

The model estimates of temperature, salinity and density (Supplementary Fig. S6) are understandably smoother after a dynamical adjustment of 18 months, though their large-scale patterns remain broadly similar to the observations. The only exception is in the subpolar gyre for the density averaged over the upper 750m, where a density increase is restricted to the northeast in the data, but spreads further west in the model due to the cyclonic circulation.

How are the uncertainties for MOC changes estimated?

To quantify the uncertainty in the MOC calculation due to errors in the estimates of the mean temperature, salinity and density fields from the observations, the following procedure was adopted:

i. The mean and standard error of density are calculated for each 1^{o}x1^{o} grid over the spatial domain at all standard depths for each of the two twenty-year periods.

ii. Monte Carlo simulations were used to estimate the mean and associated uncertainty for the MOC of each 20-year period. Specifically, a series of normally-distributed, pseudo-random values were generated for the density in each horizontal bin and at each standard depth level using the local means and standard deviations of the density field. After a selection of densities for each bin at each depth for the initialization of the model, the MOC was estimated following the integration described above. This process was repeated to produce an ensemble of estimates, the average of which provides a measure of the mean MOC and the standard deviation measure of the uncertainty of this mean. Convergence of the mean calculated from these Monte Carlo simulations required only 80 iterations.

How sensitive is our algorithm for estimating the MOC to the wind forcing?

The algorithm estimating the MOC changes between 1950-1970 and 1980-2000 (Figs. 4b and S7a) depends upon two factors: the historical changes in the densities between these two periods and the wind forcing used for the short dynamical adjustment of the model over 18 months. These competing factors are now assessed in turn. First, the MIT model is initialized with

DOI: 10.1038/NGEO947

climatological hydrographic data (averaged from 1950-2000) and forced for 18 months either by monthly NCEP winds averaged for 1950-1970 or 1980-2000. The wind-induced MOC change has a slight strengthening over the subtropical gyre and a weakening over the subpolar gyre, the opposite pattern to that previously diagnosed (Figs. S7a,b). Second, the MIT model is initialized with hydrographic data averaged either from 1950-1970 or 1980-2000 and then forced with climatological monthly NCEP winds (averaged for 1950-2000). This density-induced MOC change has a strong weakening over the subtropical gyre and a slight strengthening over the subpolar gyre, consistent with the pattern previously diagnosed (Fig. S7a,c). Hence, the inferred changes in the MOC are reliant on the imposed density changes taken from the hydrographic data, rather than the choice of the wind field used for the short dynamical adjustment. However, while the wind forcing is not important in our algorithm to estimate the MOC, the wind forcing is important in determining the density distributions, as illustrated in model assessments for the heat content and property changes for the subtropical gyre[16,34].

Do the gyre-specific overturning changes shown here also appear in isopycnal coordinates?
The gyre-specific changes in the overturning appear in isopycnal coordinates as well as depth coordinates: there is a weakening in the overturning from the former time period (1950-1970) to the latter (1980-2000) in the subtropics (Fig. S8a) and a strengthening in the subpolar region (Fig. S8b).

Supplementary References

34. Leadbetter, S.J., Williams, R.G., McDonagh, E.L. & King, B.A. A twenty year reversal in water mass trends in the subtropical North Atlantic. *Geophys. Res. Lett.* **34**, L12608-L12613 (2007).

Supplementary Figure Legends

Figure S1. Historical hydrographic data analysis at other depths. (a) Time series of the thermal (red) and haline (green) contributions to density and their sum (blue) from 1950 to 2000 averaged over the central subtropical basin, outlined in Fig. 1a, at a depth of 500 m. (b) Same as (a), except for the central subpolar basin. (c) Same as (a), except at a depth of 2000 m. (d) Same as (a), except at a depth of 2000m for the central subpolar basin. See Fig. 1b caption for further information.

Figure S2. Sampling density of the historical hydrographic data in the North Atlantic. Number of stations per 2°x2° bin for (a) 1950 to 1970 and (b) 1980-2000. 130,899 stations are available in the former time period, 239,022 in the latter. Bathymetry < 200 m is shaded gray.

Figure S3. Latitudinal pattern of density change. Density from 1980 to 2000 minus density from 1950 to 1970 as a function of latitude for selected depths. Mean density change is obtained in two ways: 1) (blue) from the sum of the mean thermal contribution (red) and mean haline contribution (green), and 2 (purple) from averaging the densities computed from individual temperature and salinity measurements. These two approaches to computing total density changes are broadly consistent. Note the mirrored pattern of the haline and thermal components,

DOI: 10.1038/NGEO947

demonstrating that density compensation is prevalent throughout the latitudinal extent of the basin. Error bars are standard errors.

Figure S4. Spatial pattern of sea surface height rise. Rate of change in sea surface height (mm yr^{-1}) evaluated between the two 20-year periods, 1980-2000 and 1950-1970 (red is an increase in sea surface height with time; blue is a decrease). (a) Data-based estimate (as in Fig. 3a). (b) Combined model and data estimate with a dynamical adjustment of 5 days. (c) As in (b), but for one year.

Figure S5. Assessment of MOC algorithm.

Change in the MOC transport (Sv) over the upper 1300 m from the latter time period of the study to the former, from an integration of the MIT model initialized with density data taken from a global inverse model, GECCO[27]: (a) Assessment of temporal adjustment with the curves varying by length of model integration, which spans from ½ year to 3 years. The 'true' MOC, diagnosed directly from GECCO monthly velocities, is designated with black crosses. The optimal timescale is for 1 year (black line). (b) Assessment of the importance of boundary data for an adjustment lasting 1 year: default (black line), truth for GECCO velocities (crosses), and with 1^{o} (blue) and 2^{o} (red) of boundary data from GECCO replaced by climatology (i.e. the long-term (1950 - 2000) average properties.) (c) As in (b) for the overturning from 100 m to 1300 m, but density data is now taken from historical data, rather than from GECCO. Note how the overturning pattern has altered when using the historical density data, compared with that diagnosed from GECCO.

Figure S6. Property changes in the model after dynamical adjustment. Model estimates of property changes between the two periods, 1980-2000 and 1950-1970, for temperature, salinity and density for the upper 750 m (left panel) and from 750 m to 1500 m (right panel). Note the greater ranges in the upper waters.

Figure S7. Attribution of MOC changes. Change in MOC (Sv) from 1950-1970 to 1980-2000 evaluated from the MIT model: (a) initialized with hydrographic data specific to each time period and integrated for 18 months with forcing by NCEP winds specific to each period (as in Fig. 4b); (b) initialized with climatological hydrographic data and monthly NCEP winds specific to each period; (c) initialized with hydrographic data specific to each period and forced by climatological monthly NCEP winds.

Figure S8. MOC change in density coordinates. Change in MOC (Sv) from 1950-1970 to 1980-2000 in density (σ_θ) coordinates, evaluated from the MIT model initialized with historical hydrographic data from these two time periods for (a) a representative subtropical latitude and (b) a representative subpolar latitude.

DOI: 10.1038/NGEO947

Figure S1

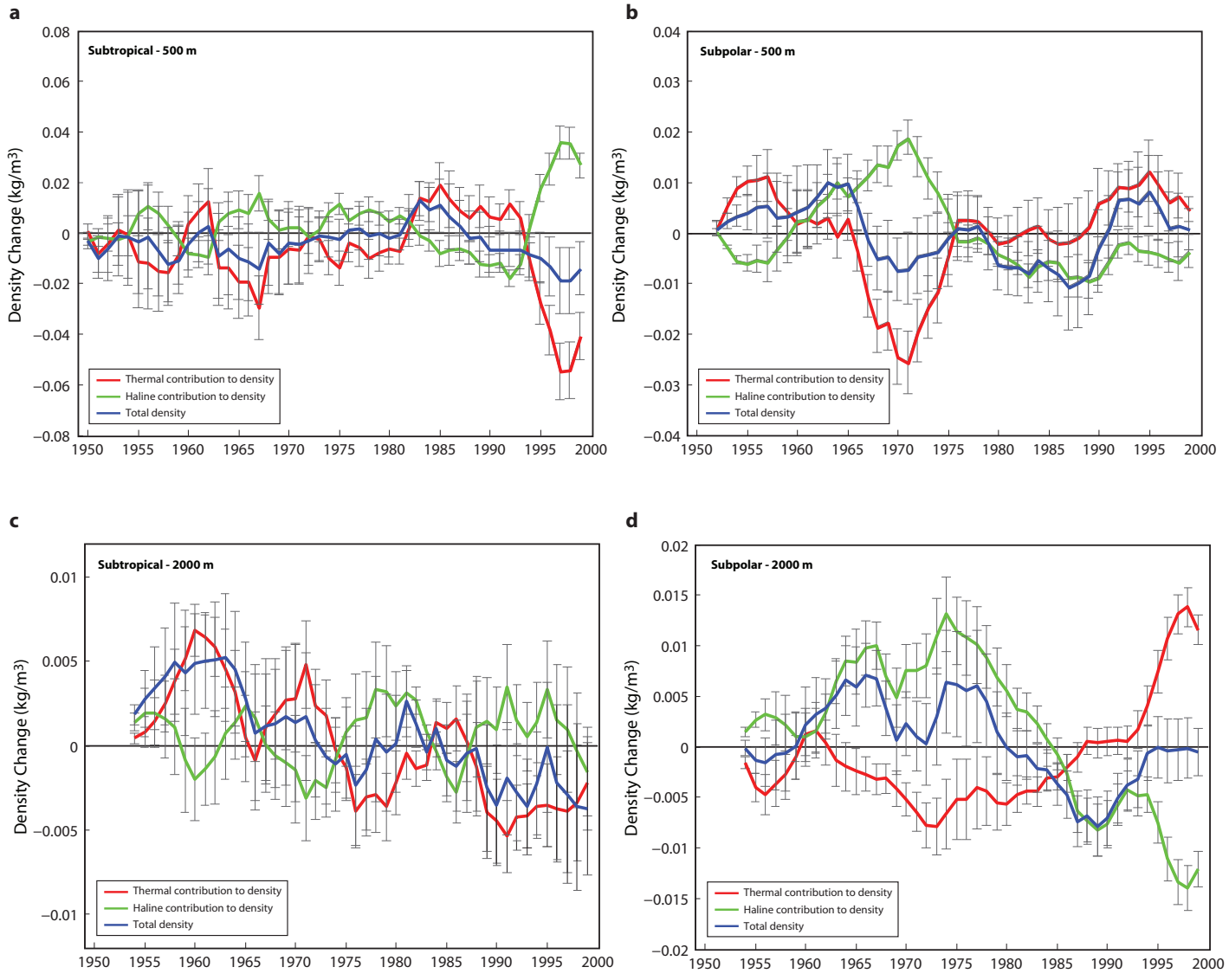

Figure S2

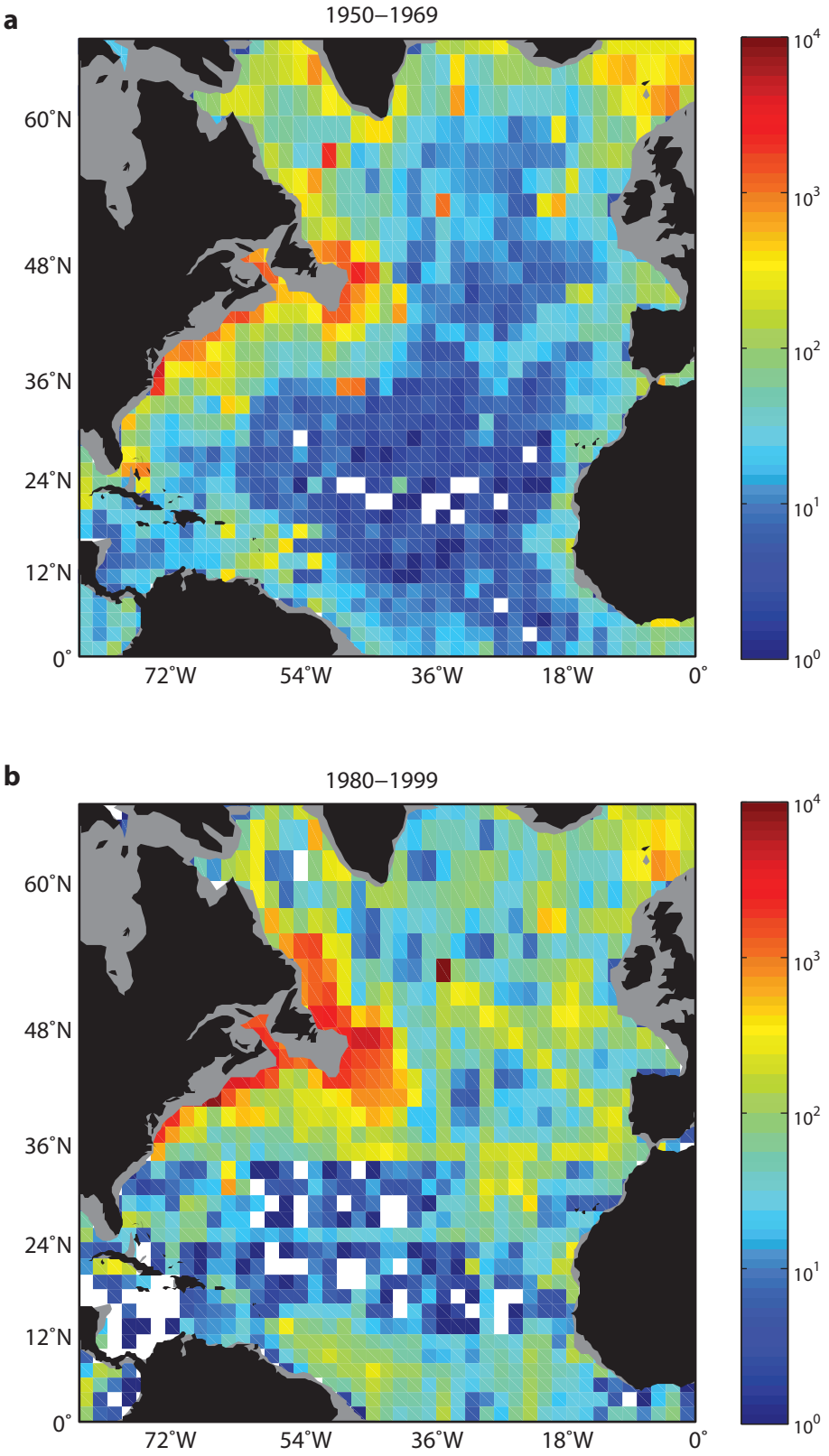
a
1950–1969
60°N
48°N
36°N
24°N
12°N
0°
72°W
54°W
36°W
18°W
0°
10^4
10^3
10^2
10^1
10^0
b
1980–1999
60°N
48°N
36°N
24°N
12°N
0°
72°W
54°W
36°W
18°W
0°
10^4
10^3
10^2
10^1
10^0

DOI: 10.1038/NGEO947

Figure S3

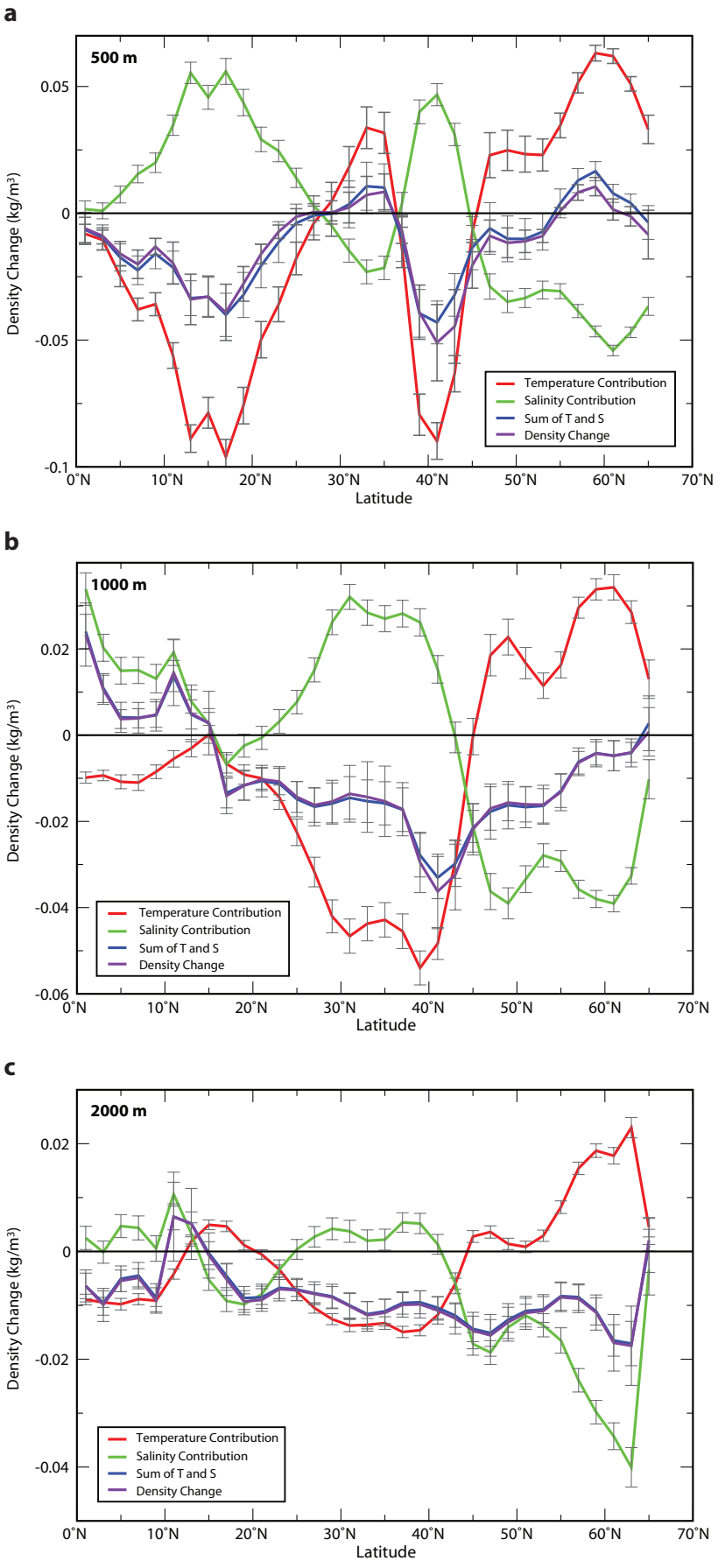

Figure S4

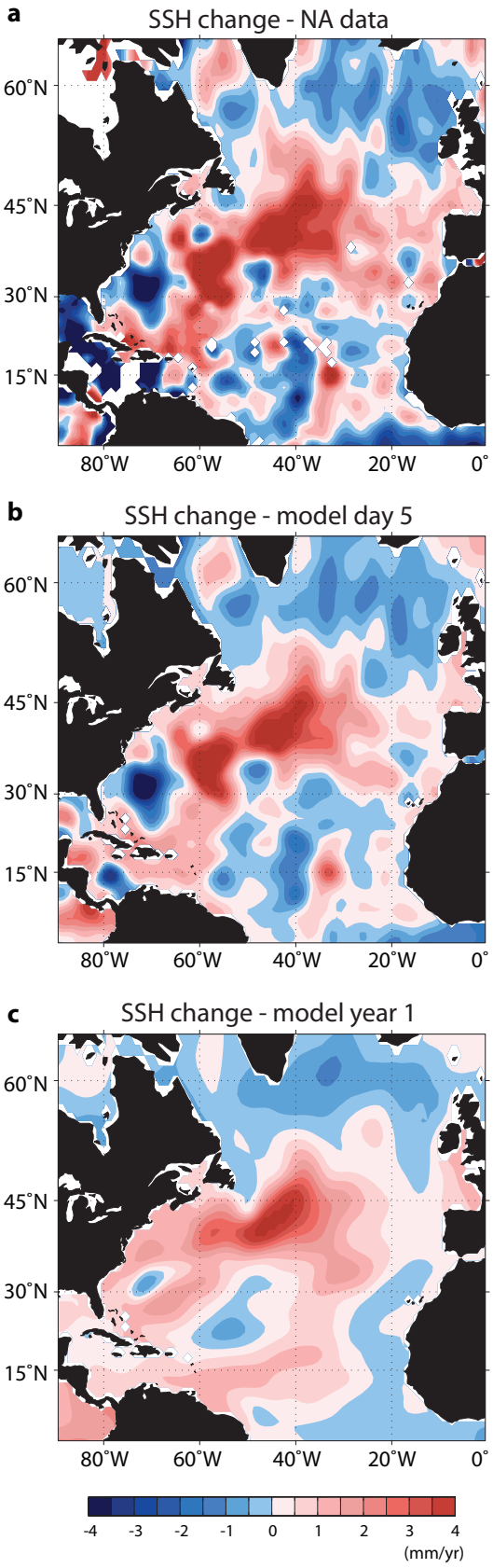
a
SSH change - NA data
60°N
45°N
30°N
15°N
80°W
60°W
40°W
20°W
0°
b
SSH change - model day 5
60°N
45°N
30°N
15°N
80°W
60°W
40°W
20°W
0°
c
SSH change - model year 1
60°N
45°N
30°N
15°N
80°W
60°W
40°W
20°W
0°
-4
-3
-2
-1
0
1
2
3
4
(mm/yr)

DOI: 10.1038/NGEO947

Figure S5

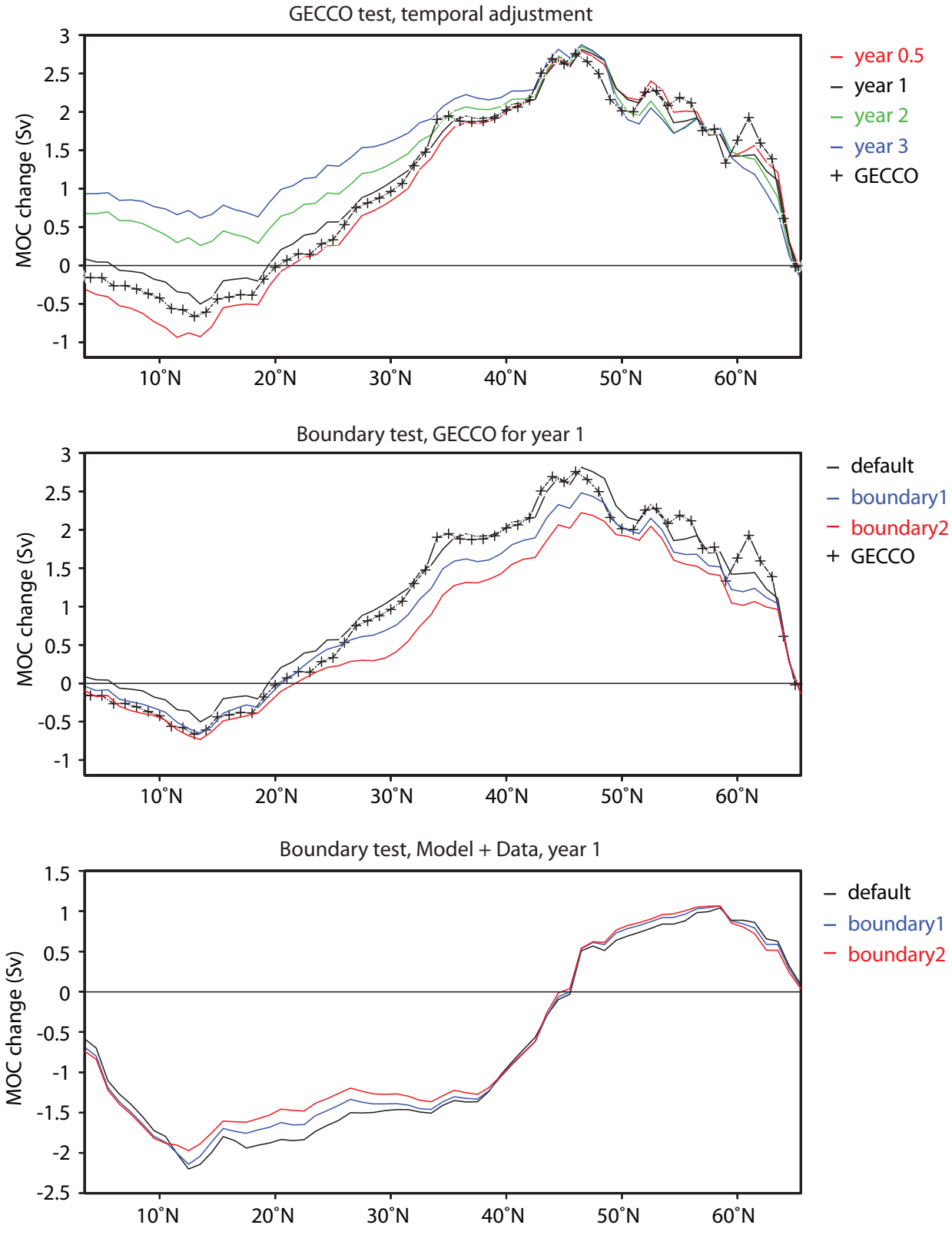

Figure S6

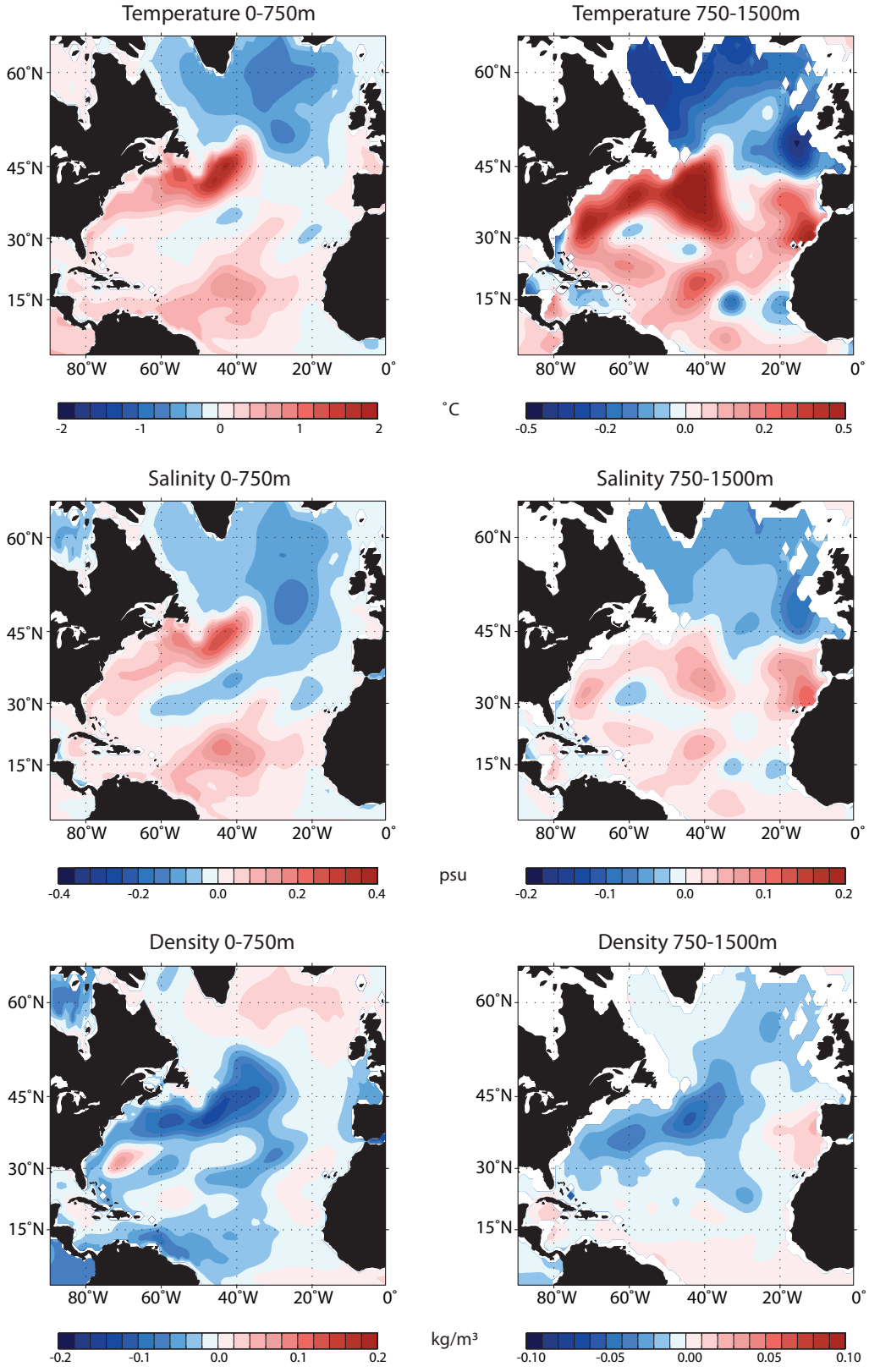
Temperature 0-750m
Temperature 750-1500m
60°N
45°N
30°N
15°N
80°W
60°W
40°W
20°W
0°
-2
-1
0
1
2
°C
-0.5
-0.2
0.0
0.2
0.5
Salinity 0-750m
Salinity 750-1500m
-0.4
-0.2
0.0
0.2
0.4
psu
-0.2
-0.1
0.0
0.1
0.2
Density 0-750m
Density 750-1500m
kg/m³
-0.10
-0.05
0.00
0.05
0.10

DOI: 10.1038/NGEO947

Figure S7

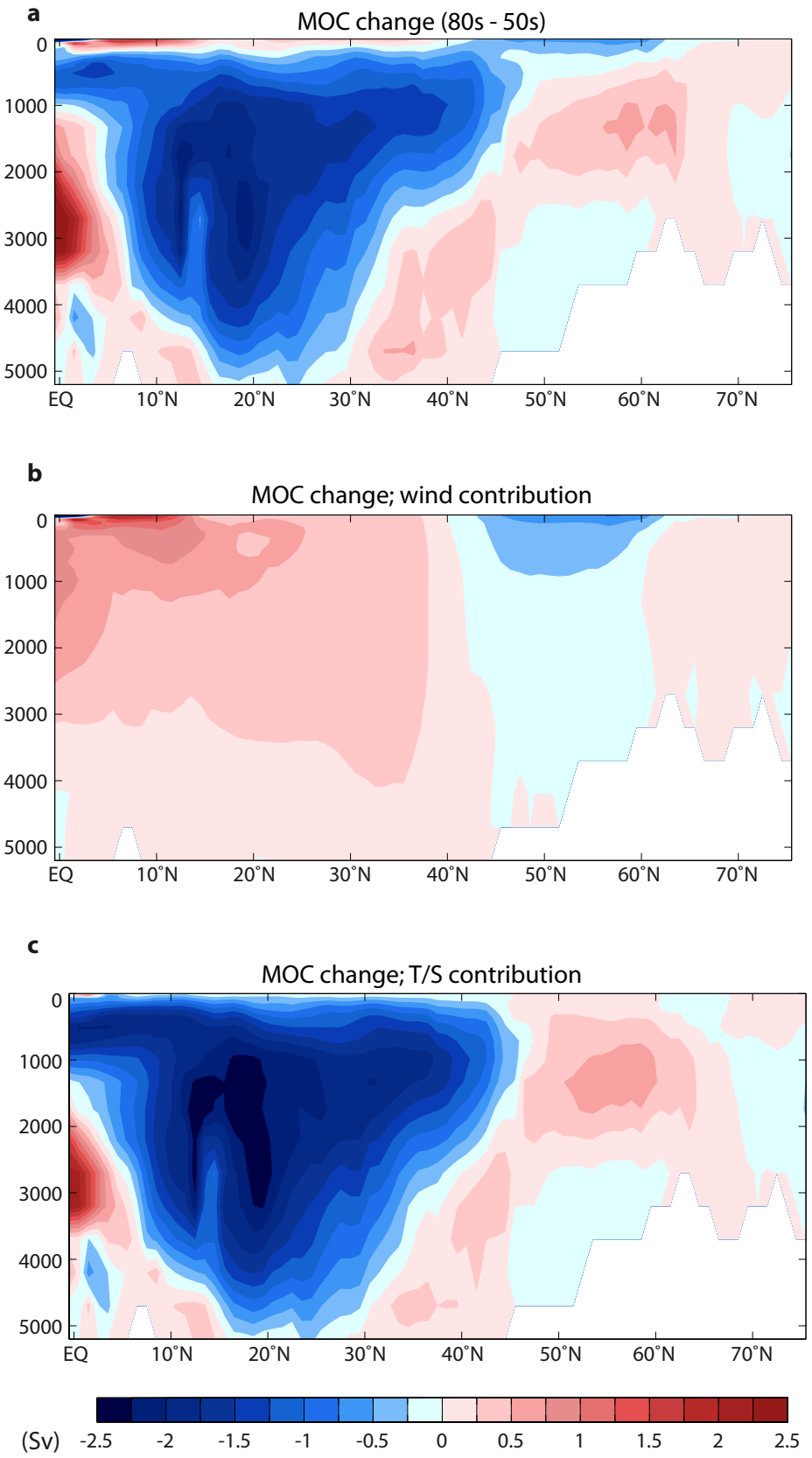

Figure S8

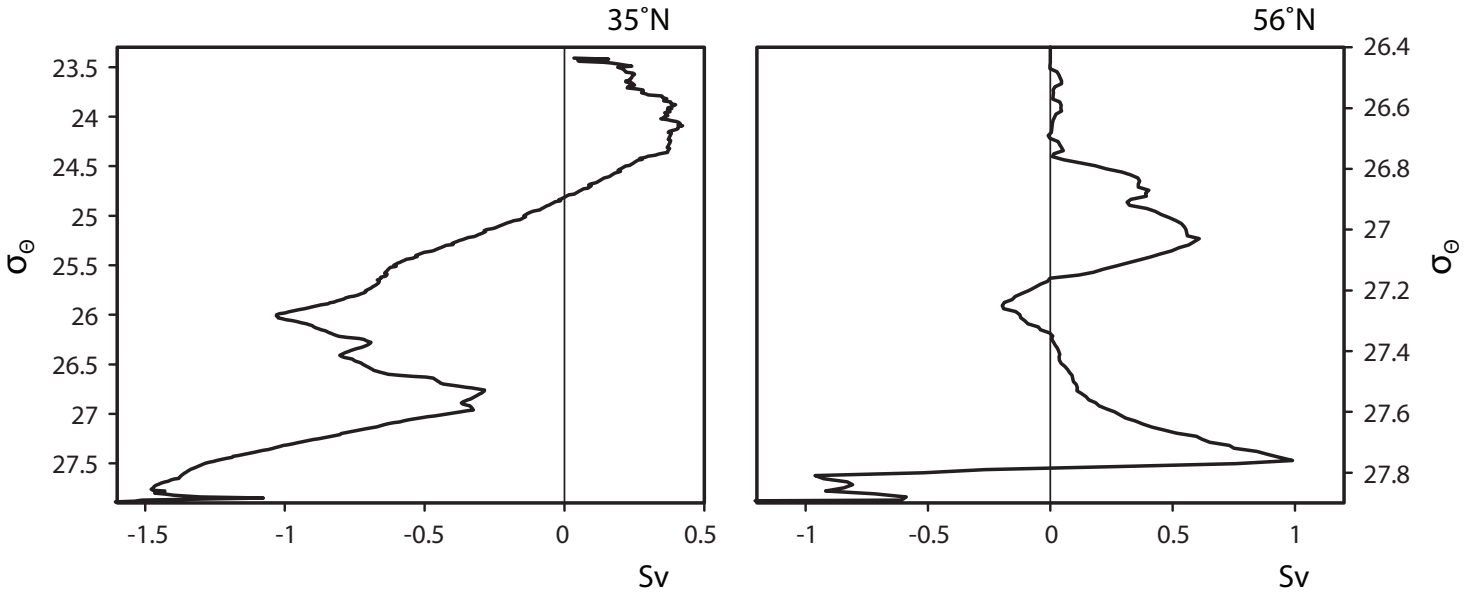
35°N
56°N
23.5
24
24.5
25
25.5
26
26.5
27
27.5
σΘ
-1.5
-1
-0.5
0
0.5
Sv
26.4
26.6
26.8
27
27.2
27.4
27.6
27.8
σΘ
-1
-0.5
0
0.5
1
Sv